American Journal of Heterocyclic Chemistry
2026, Vol. 11, No. 2, pp. 22–36
https://doi.org/10.11648/j.ajhc.20261102.11

Research Article

Influence of the Central Metal Ion on the Physicochemical Properties of a Water Soluble Series of Silver Nanoparticles/Metallophthalocyanines (Fe, Co, Ni, Cu) Hybrids

Lassane Tarpaga[1, *], Wend Kuny Guy Aristide Nitiema[1], Seydou Ouedraogo[1], Youssoufou Bakouan[1], Bintou Sessouma[1], Mabinty Bayo Bangoura[1], Catherine Amiens[2], Karifa Bayo[1]

[1]Laboratory of Molecular Chemistry and Materials, Joseph KI-ZERBO University, Ouagadougou, Burkina Faso
[2]Toulouse University, CNRS-LCC, Toulouse, France

Abstract

This work reports the synthesis and characterization of nanostructured hybrid systems based on the combination of water soluble transition-metal phthalocyanines of a Fe, Co, Ni, and Cu, and silver nanoparticles (AgNPs). Transmission electron microscopy reveals images of the hybrid compounds, which are approximately 20 nm in size. The bathochromic shift and the broadening of the plasmon band characteristic of AgNPs, observed in the UV-Vis spectra of the nanostructured hybrid systems, indicate the coordination of the complexes on the nanoparticle surface. Infrared and Raman spectra confirmed an effective interaction between the complexes, and the nanoparticles, marked in particular by a modulation of intensities and shifts in characteristic frequencies. Raman spectroscopy identified a SERS (surface-enhanced Raman scattering) effect due to the plasmonic resonance properties of the AgNPs. The shifts observed for the C-N-C bond follow a clear trend related to the ionic radius and the polarizing power of the metals. Solid-state NMR ^{13}C CP-MAS, an innovative tool for these types of compounds, yields results consistent with those obtained for nanohybrids systems comprising Zn phthalocyanine complexes. All these results indicate the formation of nanohybrid species, and suggest that they may be good candidates for various applications, such as photocatalysis.

Keywords

Metallophthalocyanine**,** Nanoparticles, Nanohybrid, Characterization

1. Introduction

Since their accidental discovery, metallophthalocyanines (MPcs) have established themselves as indispensable macrocycles in modern chemistry, evolving from simple industrial pigments to sophisticated molecular building blocks for nanotechnology. Indeed, the delocalization of the eighteen π electrons and their highly conjugated structure endow MPcs with

*Correspondence: Lassane Tarpaga (lassanetarpaga@yahoo.com), Lassane Tarpaga (lassane.tarpaga@ujkz.bf)

Received: 14 October 2026; **Accepted:** 26 October 2026; **Published:** 11 November 2026

Copyright: © The Author(s), 2026. Published by Science Publishing Group. This is an **Open Access** article, distributed under the terms of the Creative Commons Attribution 4.0 License (http://creativecommons.org/licenses/by/4.0/), which permits unrestricted use, distribution and reproduction in any medium, provided the original work is properly cited.

electron-transfer capabilities, excellent absorption across a broad range of the visible spectrum, and redox [1], optical [1, 2], conductive [3], electrochemical [4], and luminescent [5] properties. Their thermal [6] and chemical stability makes them sublimable and crystallizable, which allows for the production of high-purity materials. However, the study of MPc and their applications generally requires sufficient solubility in common solvents, which is often a challenge given the considerable intermolecular cohesive forces between the macrocycles [7]. These cohesive forces can nevertheless be controlled through appropriate functionalization at the periphery of the phthalocyanines with solubilizing chains bearing carboxyl, anhydride, or amide groups, which can allow for fine-tuning of the physicochemical properties, particularly solubility and the tendency to aggregate. Moreover, the introduction of functional groups onto these macrocycles may open up a new avenue, allowing for the adjustment of intermolecular interactions with metal center (M) and also by exploiting intermolecular hydrogen bonds. This network of hydrogen bonds also stabilizes the arrangement of the MPc on surfaces, among which nanoparticles (NPs) surfaces, preventing disordered aggregation that would mask signals in vibrational spectroscopy (infrared and Raman). The formation of hybrid species with NPs [8-15] represents one of the major innovations of recent years in the field of MPc chemistry. In particular, MPc@silver nanoparticle hybrid systems have been studied as potential antibacterial agents or photosensitizers [16].

For example, the work by Sumam V. et al. on the photophysical properties of a hybrid species consisting of a zinc phthalocyanine ($ZnPc(SH)_8$, Figure 1A) conjugated with silver nanoparticles (AgNPs), noted $[ZnPc(SH)_8]$@AgNPs, demonstrated a great improvement in these properties following conjugation compared to the two individual entities [17]. Synergistic—or at least cumulative—effects between MPc and AgNPs are therefore thought to occur in these hybrids. However, the solubility of the $[ZnPc(SH)_8]$@AgNPs hybrid was relatively low, and the particles exhibited significant aggregation as observed by electron microscopy. Furthermore, while the overall architecture of the MPc is well understood, and some MPc@NPs have been developed, the specific influence of the metal center, M, on the coordination of these MPcs on the surface of NPs remains a subject of debate.

Recently, we introduced the combination of two factors that lead to the formation of water-soluble complexes with anchoring functionality (Figure 1B). The first factor is the introduction of -COOH groups at the periphery of the macrocycle to render the compounds soluble, and the second is the introduction of thiol (-SH) groups that serves as attachment sites for silver nanoparticles. This synthetic strategy led to the successful synthesis of ZnPc@AgNPs nanohybrids of improved water solubility [18]. In this article, we extend the scope of this synthetic strategy and report the synthesis, and spectroscopic and microscopic characterization, of a series of nanohybrids comprising transition-metal phthalocyanines (Fe, Co, Ni, and Cu) linked to AgNPs and compare the effect of coordination depending on the central metal of the MPc.

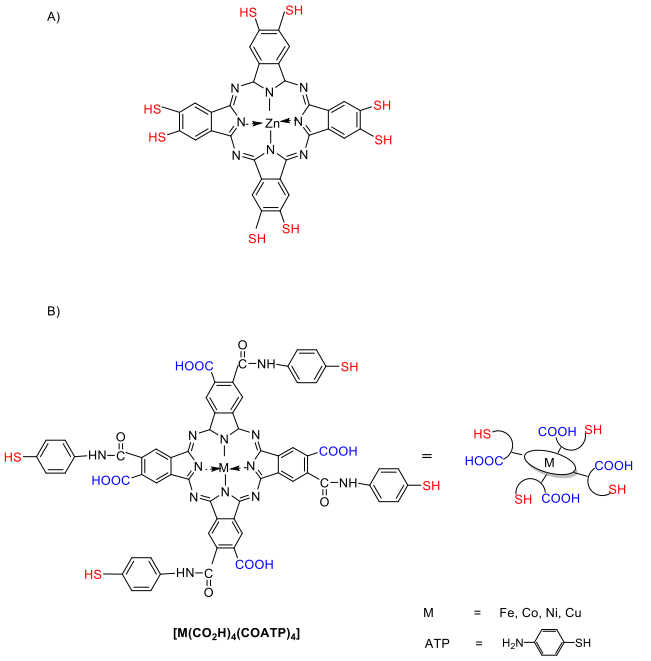


Figure 1. *A) zinc complex described in the literature [17], and B) amide complexes used in this study: $[MPc(CO_2H)_4(COATP)_4]$, with M = Fe, Co, Ni, Cu and ATP = 4-aminothiophenol, and their schematic representation.*

2. Experimental

2.1. Materials

Pyromellitic dianhydride ((> 97%, Sigma Aldrich), nickel (II) acetate tetrahydrate ((> 99%, Sigma Aldrich), copper (II) chloride dihydrate ((> 99%, Sigma Aldrich), cobalt(II) acetate tetrahydrate (> 99%, Sigma Aldrich), iron(II) sulfate heptahydrate (> 99%, Sigma Aldrich), urea (99%, Sigma Aldrich), ammonium heptamolybdate tetrahydrate (> 99%, Sigma Aldrich), nitrobenzene (> 99%, Sigma Aldrich), toluene (> 99.9% Alfa Aesar), methanol (> 99.9%, Alfa Aesar), acetone (> 99.9%, Alfa Aesar), sodium hydroxide (NaOH) (≥ 98%, Sigma Aldrich), hydrochloric acid (37%, Sigma Aldrich), acetic anhydride (> 99.5%, Sigma Aldrich), 4-aminothiophenol (ATP) (>97%, Sigma Aldrich), 4 Å molecular sieve (99%, Sigma Aldrich), silver nitrate (>98%, Alfa Aesar), ethylenediaminetetramethylenephosphonic acid (EDTMP, > 99%, Alfa Aesar), ammonia solution (> 25%, Alfa Aesar), dimethylformamide (DMF, 99%, Thermo Fisher Scientific). Ultrapure water was produced using a Milli-Q system from Millipore (MQ, 18.2 MΩ). Unless otherwise specified, all reagents and solvents were used without further purification.

2.2. Synthesis

2.2.1. Preparation of amide metallophthalocyanines [MPc(CO$_2$H)$_4$(COATP)$_4$] with M = Fe, Co, Ni, Cu

We prepared and purified the acid form of the [MPc(CO$_2$H)$_8$] complexes as described in the literature [19]. This less reactive acid form was converted to an anhydride intermediate [MPc(C$_2$O$_3$)$_4$] under a dry argon atmosphere, given the high reactivity of the products toward trace amounts of water. All amide complexes were obtained adapting the method published in Tarpaga et al [18]. Namely, a mixture of 0.1 g (10^{-4} mol) of [MPc(C$_2$O$_3$)$_4$] and 0.2 g (10^{-3} mol) of 4-aminothiophenol in 10 mL of dry DMF was maintained at 70 ℃ for 3 days. At the start of heating, the reaction mixture was dark green in color. At the end of the synthesis, the resulting mixture was cooled down to room temperature; the product was precipitated in 20 mL of dichloromethane and then recovered by filtration. The isolated solid was washed thoroughly with dichloromethane and then with acetone, and dried in air. A black powder was obtained with an average yield of 80% (Figure 2). These complexes were all characterized using modern characterization techniques prior to the synthesis of the hybrid species. Variations in the nature of the central metal ion slightly influence certain properties of the complexes, but overall, the following results were obtained: *[FT-IR (ATR) ν_{max}/cm^{-1}: 727 (C-H), 1570 (N-H amide), 1715 (C=O amide); Raman ν_{max}/cm^{-1}: 645 (C-S aryl), 682 (β_{C-H}), 745 (δ_{C-H} pyrrole), 1500 (C=N); RMN ^{13}C (solid state) δ/ppm: 165.2 (-CONH), 149.5 (C_B), 117.5 (C_{ATP}); UV-Visible λ/nm: DMF (710, Q; 368, B); DMSO (711, Q; 375, B)]*.

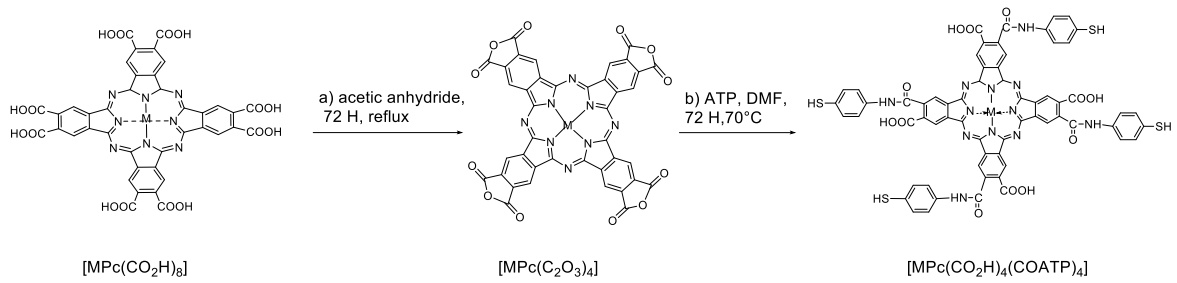


Figure 2. *Reaction scheme for the synthesis of the amide complexes [MPc(CO$_2$H)$_4$(COATP)$_4$], M = Fe, Co, Ni, Cu.*

2.2.2. Preparation of Silver Nanoparticles (AgNPs)

Silver nanoparticles (AgNPs) were prepared by reducing a silver nitrate solution according to the method described in the literature [20]. The reaction scheme is shown in Figure 3. Briefly, an aqueous solution of $AgNO_3$ (1.23 mM, 25mL), adjusted to pH = 8.5 using a commercial ammonia solution, was placed in a 50 mL flask and refluxed for 10 min. To this boiling solution, kept under vigorous stirring, 160 µL of an aqueous (0.19 M) EDTMP solution was rapidly added. Heating was stopped after 20 min, but stirring was maintained until the medium returned to room temperature. The final solution obtained was stored under argon (7 ℃). The characteristic plasmon band wavelength of AgNPs in solution (Water, DMF) was observed at λ = 400 nm, the average size was determined by TEM: 17 +/- 4 nm.

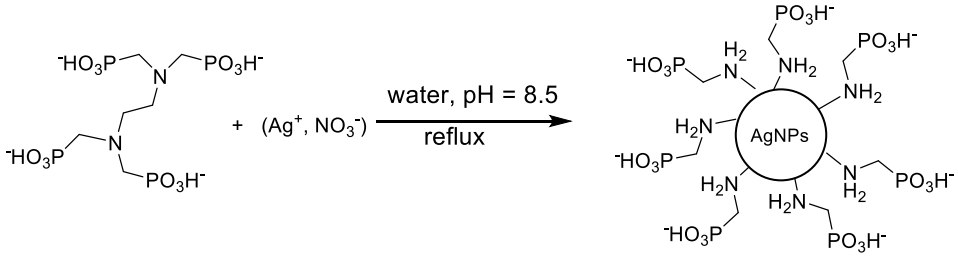


Figure 3. *Reaction scheme for the synthesis of AgNPs.*

2.2.3. Preparation of Hybrid Species [MPc(CO$_2$H)$_4$(COATP)$_4$@AgNPs]; M = Fe, Co, Ni, Cu

We synthesized and purified the hybrid species as described in previous work by Tarpaga et al. [18]. The synthesis strategy is reported in Figure 4. Namely, to 50 mL of a solution of AgNPs (≈ 0.01 µmol), an excess (3.5 µmol) of the complex dissolved in DMF (50 mL) was added; then the mixture was stirred for 72 h at 25 ℃. The mixture took on a dark green color that persisted until the end of the reaction. An aliquot (40 mL) was washed by centrifugation with a mixture of solvents (1:1 DMF-Milli-Q water). The operation was repeated 3 times. During the last cycle, 30 mL of supernatant was discarded and the remaining solution was freeze-dried. At the end of this final phase, a black powder was obtained (8.5 mg, 13mg, 10mg and 11mg for the Fe, Co, Ni and Cu derivatives, respectively).

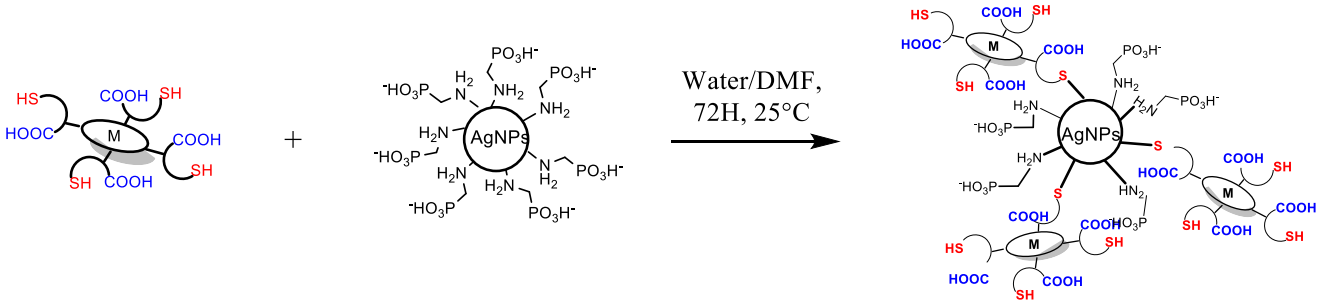


Figure 4. *Strategy for synthesizing the nanohybrid species.*

2.3. Equipment

2.3.1. Optical Absorption Spectroscopy

The UV-visible spectra of compounds dissolved in DMF or in a water-DMF mixture (50/50) were recorded using a 190 DES (Double Energy System) spectrometer, thereby allowing interesting comparisons with data from the literature.

2.3.2. Infrared and Raman Absorption Spectroscopy

The IR spectra were recorded from the sample powders using a Brucker TENSOR 27 type spectrometer, ATR diamond. The RAMAN spectra were obtained with the same powders of the samples. The Raman spectrometer (HoribaJobin Yvon HR800) with a 638 nm wavelength laser was used for spectral acquisition.

2.3.3. Transmission Electron Microscopy (TEM)

The study was carried out at the Raimond Castaing Microcharacterization Center (Toulouse). Conventional TEM images were recorded on a JEOL JEM 1400 microscope Samples were prepared by depositing a drop of the diluted colloidal solution on a copper grid covered with a thin film of carbon, followed by air drying and then drying under high vacuum. Average sizes were determined after counting a minimum of 250 particles using Image J software.

2.3.4. Solid-State ^{13}C Nuclear Magnetic Resonance (^{13}C NMR)

The samples were characterized using a Bruker Avance 400 III HD spectrometer operating at a magnetic field of 9.4 T. The samples were loaded into 3.2-mm zirconia rotors and centrifuged at 10 kHz at 298 K. The ^{13}C CP (Cross-Polarization) MAS (Magic Angle Spinning) NMR spectra were recorded with a recycle time of 2 s and a dwell time of 2 ms. The chemical shifts were referenced to TMS. The ^{13}C chemical shift assignments for our samples were made by analogy with previous work published in the literature on similar complexes [21-23].

3. Results and Discussions

3.1. Transmission Electron Microscopy (TEM)

TEM images of AgNPs (Figure 5) show that the particles are spherical with an average diameter of 17 +/- 4 nm. This result is consistent with those reported by Chaikin, Y, et al. [20].

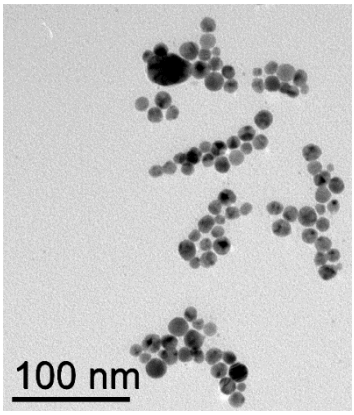


Figure 5. *TEM image of AgNPs, scale bar: 100 nm.*

A typical TEM image of the Co hybrid species is shown in Figure 6, as a representative example, while TEM images of the Fe, Ni and Cu derivatives are reported in Figure 7. The images show NPs with an average size of approximately 20 nm that are more uniformly dispersed compared to those described in the literature [17, 24, 25] regarding MPcs@AgNPs hybrids.

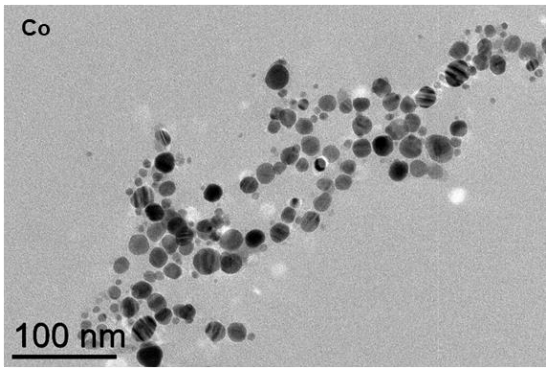


Figure 6. *TEM image of [CoPc(CO$_2$H)$_4$(COATP)$_4$@AgNPs].*

A plausible explanation may lie in the unique nature of the series of amide complexes we prepared. Indeed, thanks to their four thiol groups, the complex would bind more readily to the surface of the NPs, thereby minimizing the π-π interactions that most often cause aggregation of these types of hybrid species [15]. Similarly, the presence of carboxylic acid groups could account for the good dispersion of the hybrid compound in solution; since these groups are deprotonated at the reaction pH—and even in milli-Q water—electrostatic repulsions arise between the NPs, thereby promoting better dispersion. These results are thus first proof, although indirect, of a successful interaction between the MPc complex and the AgNPs.

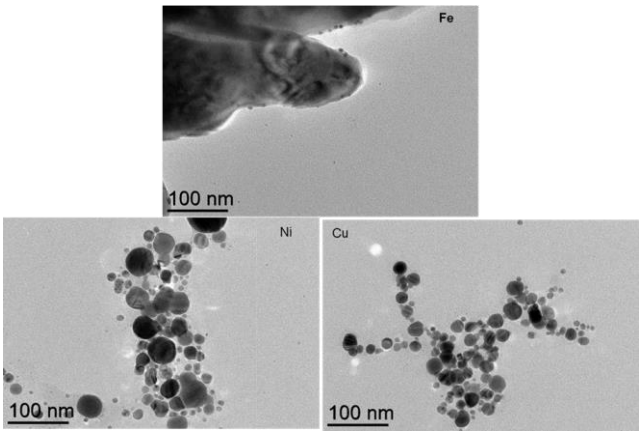


Figure 7. *TEM image of [MPc(CO$_2$H)$_4$(COATP)$_4$@AgNPs], M = Fe, Ni and Cu.*

3.2. UV-Visible Spectroscopy

The parent [MPc(CO$_2$H)$_4$(COATP)$_4$] complexes display UV-vis spectra typical of MPc complexes of Fe, Co, Ni and Cu notably the presence of the two main bands [19].

Electron absorption spectroscopy is a useful tool for characterizing metal NPs due to the presence of a characteristic plasmon band. Above all, it provides information about their local environment.

The plasmon band of the hydrid is observed at 422 nm, 419 nm, 407 nm, and 411 nm, in the spectra of Fe, Co, Ni, and Cu derivatives, respectively.

When comparing to the spectrum of the primary AgNPs, which display a plasmon band at 390 nm, a bathochromic shift of 17 to 32 nm is evidenced upon thiol binding (Figure 8). According to previous studies, this shift toward longer wavelengths may be related to the functionalization of the nanoparticle surface [15, 16]. In that respect, Riya J. et al. [24] obtained similar results when they studied AgNPs bound to L-tyrosine, and Sumam V. et al. observed a shift of approximately 50 nm in the spectra of the ZnPc(SH)$_8$@AgNPs hybrid species [17].

However, the shift is accompanied by a broadening of the peak, which suggests a change in the size or organization of the nanoparticles in solution.

Comparing the UV-vis spectrum of the hybrid with the one of the parent MPc complex, shows that the characteristic band of the complex in the 550-750 nm region is only slightly altered by the reaction, as already observed in the case of the ZnPc-AgNPs nanohybrid. [18] It shifts from 703 nm to 710 nm in the spectrum of the FePc-AgNPs derivative. A similar result is obtained with Co, and Ni derivatives. Concerning the Cu derivative, the low absorption in the 550-750 nm region doesn't allow to draw any firm conclusion.

Overall, our results are consistent with data from the literature and support the coordination of the MPc via their thiol groups at the particle surface.

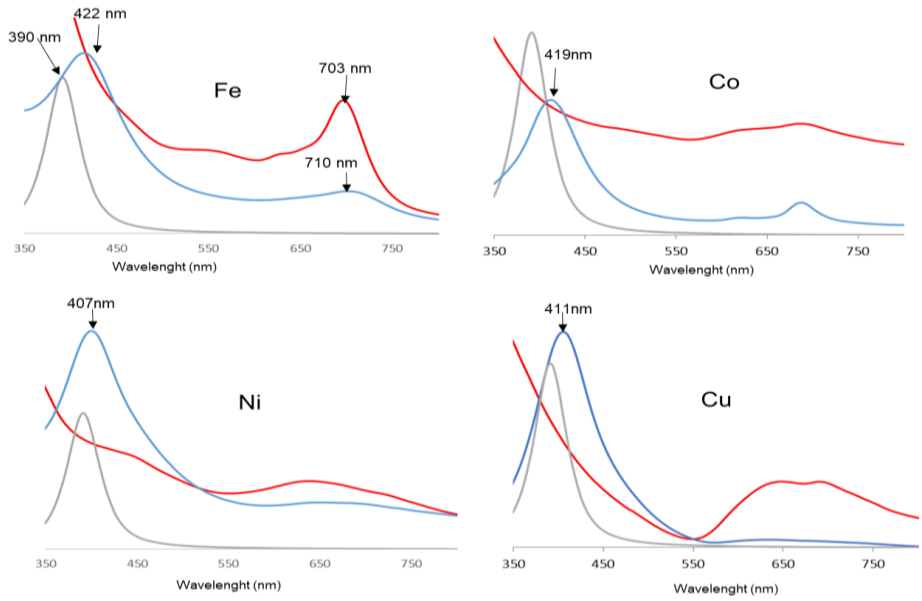


Figure 8. *UV-Vis spectra of the parent [MPc(CO₂H)₄(COATP)] complexes (red line), AgNPs (grey line) and [MPc(CO₂H)₄(COATP)₄@AgNPs] hybrids (blue line), M = Fe, Co, Ni, Cu.*

3.3. Infrared and Raman Vibrational Spectroscopy

The IR spectra of the [MPc(CO₂H)₄(COATP)₄] complexes and [MPc(CO₂H)₄(COATP)₄@AgNPs] nanohybrids were recorded to investigate the interaction between the two entities and evidence any possible effect of the nature of the central metal of the amide complexes. The spectra of the Co derivatives are given in Figure 9, as typical examples of the series, while IR spectra of the Fe, Ni and Cu derivatives are reported in Tables 1 and 2, which list the positions and intensities of the main peaks of the IR spectra of all new derivatives prepared in this work.

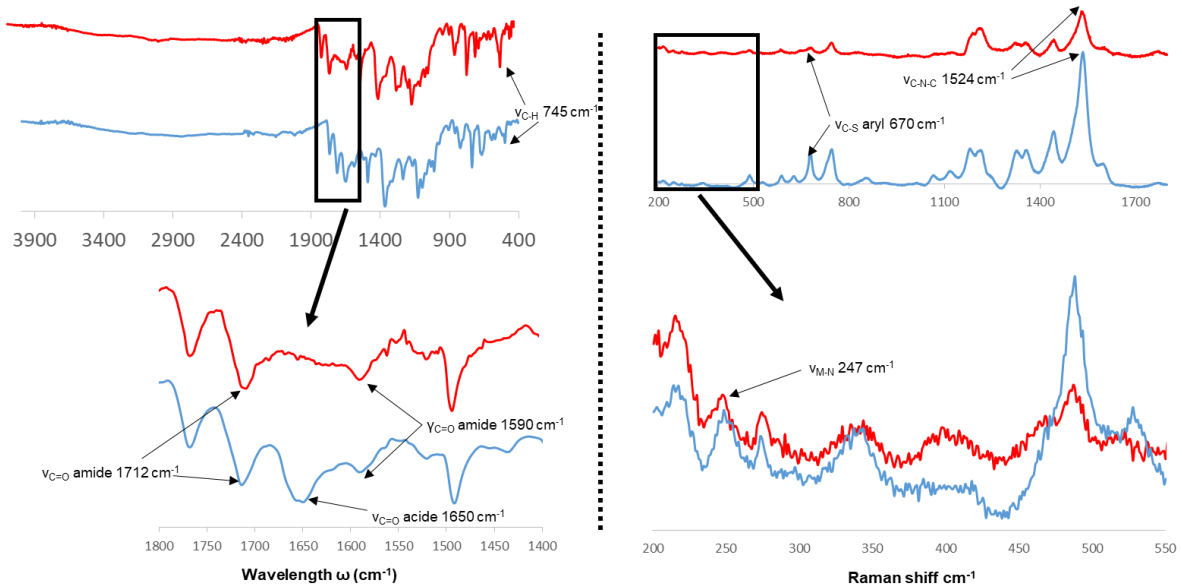


Figure 9. *IR (left) and Raman (right) spectra of [CoPc(CO₂H)₄(COATP)₄] (red line) and [CoPc(CO₂H)₄(COATP)₄@AgNPs] (blue line).*

The relative intensity of the νC-H band at circa 750 cm^{-1} in the spectra of [MPc(CO₂H)₄(COATP)₄] decreases only slightly across the spectra of the various complexes. Depending on the central metal, this band is shifted toward higher frequencies in the order Fe > Co > Ni > Cu (740, 745, 747 and

748 cm^{-1}, respectively). Between 1300 and 2000 cm^{-1}, the main observation is the perturbation of the νC=O vibrational band. It is observed between 1696 and 1722 cm^{-1} in all spectra of the MPc. It does not follow a specific pattern. Moreover, in the case of cobalt, the νC=O band of the carboxylic acid groups which was not observed in the spectrum of the free amide complex is strongly influenced by coordination; it is observable at 1650 cm^{-1} in the spectrum of [$CoPc(CO_2H)_4(COATP)_4$@AgNPs].

In the spectra of amide complexes and hybrid species, the band at circa 1712cm^{-1}, which is absent from the spectrum of the non-functionalized MPc, $MPc(CO_2H)_4(COATP)$, is attributable to a deformation vibration of the amide νC=O functional group, analogous to that reported in the literature [26, 27]. This band is independent of the central metal, both in the MPc and in the MPc@AgNPs hybrids, M = Fe, Co, Ni and Cu [18].

In the IR spectra of the hybrid species, a notable feature is the modulation of the relative intensities of the vibration bands of the MPc entity in the hybrid, in comparison to the free MPc. The hybrid species [$MPc(CO_2H)_4(COATP)_4$@AgNPs] exhibit a disappearance of certain peaks related to C=C or C-H vibrations, and a shift in the characteristic peaks relative to those of the amide complexes [$MPc(CO_2H)_4(COATP)_4$]. This can be explained by the strong and effective interaction between the amide complexes and the AgNPs.

Variations in the central metal in the MPc do not have a significant effect on most vibrational frequencies, as evidenced by the similar frequencies observed for the same vibrational mode. It is even the case for the medium-intensity bands observed around 900 cm^{-1} which, according to Kobayashi et al. [28], are associated with metal-ligand vibrations (here M-N bonds). However, in the spectra of [$MPc(CO_2H)_4(COATP)_4$@AgNPs], this M-N vibration band around 900 cm^{-1}, shifts by approximately 10 cm^{-1} toward higher frequencies in the order Fe, Co, Ni, and Cu (ΔE = 8, 15, 9 and 27 cm^{-1}, respectively). This can be explained by the change in the macrocycle's electron density due to the interaction of delocalized π-electrons with the AgNPs. A similar peak shift has been reported for phthalocyanine-stabilized gold and copper nanoparticles [28, 29]. Our infrared analysis, confirms that these bands measure the strength of the interaction between the metal and the ligand.

Table 1. *Characteristic IR vibration bands in cm^{-1} of Fe and Co compounds.*

[$FePc(CO_2H)_4(COATP)_4$]	**[$FePc(CO_2H)_4(COATP)_4$@AgNPs]**	**[$CoPc(CO_2H)_4(COATP)_4$]**	**[$CoPc(CO_2H)_4(COATP)_4$@AgNPs]**	**Attributions**
3600-2260 l	3600-2250 l	3600-2350 l	3600-2356 l	ν_{O-H}
1768 F	1770 F	1767 F	1768 F	$\nu_{C=O}$
1714 F	1716 F	1710 F	1720 F	
1648 F	1652m		1650 F	$\nu_{C=N}$
1590 f	1591 f	1589 m	1590 f	$\gamma_{C=O}$
1492 F	1492 m	1519 f	1518	$\nu_{C=C}$
		1491 F	1492 F	ν_{C-H}
1372 F	1376 m	1365 F	1366 F	ν_{C-O}
1216 f	1250 m	1236 F	1236 F	
		1168 f	1142 f	ν_{C-N}
1122 F	1156 F	1126 m	1128 F	
1030 F	1012 F	1033 m	1098 m	
1010 m	??1008f	1011f	1012 m	
915m	923 m	905 m	920 f	M-N
824 m	806 m	822 m	824 m	
740 m	747 m	745 F	748 F	ν_{C-H}
680 m	685 m	677 m	666 m	
668 f	665f	652 m	594 m	
550 m	574 m	500 F	500 m	

[FePc(CO$_2$H)$_4$(COATP)$_4$]	[FePc(CO$_2$H)$_4$(COATP)$_4$ @AgNPs]	[CoPc(CO$_2$H)$_4$(COATP)$_4$]	[CoPc(CO$_2$H)$_4$(COATP)$_4$@AgNPs]	Attributions
498 f	500 m	433 m	458 f	ν_{C-C}
458 m	442 f	421 f	420f	deformation of the macro-cycle

Table 2. Characteristic IR vibration bands in cm^{-1} of Ni and Cu compounds.

[NiPc(CO$_2$H)$_4$(COATP)$_4$]	[NiPc(CO$_2$H)$_4$(COATP)$_4$@AgNPs]	[CuPc(CO$_2$H)$_4$(COATP)$_4$]	[CuPc(CO$_2$H)$_4$(COATP)$_4$@AgNPs]	Attributions
3600-2345 l	3600-2340 l	3600-2500 l	3600-2356 l	ν_{O-H}
		1772 m	1775 m	$\nu_{C=O}$
1722 m	1714 F	1720 m	1716 F	
1600 F	1650 F	1650 F	1660 m	$\nu_{C=N}$
1552	1594 F	1566	1590 F	$\gamma_{C=O}$
1492 m	1492 F			
1436 m	1437 m	1492 m	1492 F	$\nu_{C=C}$
1384 F	1370 F	1364 F	1364 F	ν_{C-H}
1310 m	1310 F			
1252 m	1250 f	1236 m	1240 F	ν_{C-O}
1150 f	1128 f	1124 f	1126 F	ν_{C-N}
1092 m	1095 m	1099 F	1098 f	
		1080 f	1066 m	
	1012 m		1014 F	M-N
921m	930 m	921m	948 f	
	818 m	826 f	828 f	
747 m	750 m	748 m	753 F	ν_{C-H}
658 F	636 m	658 m	670 m	
	594 f		596 f	
502 f	516 f	514 f	512 m	ν_{C-C}
	458 f	460 f	490 m	deformation of the macro-cycle
	418 f		400 f	

A complementary study was carried out using Raman spectroscopy. Figure 9, right, presents the Raman spectra of the cobalt derivatives, [CoPc(CO$_2$H)$_4$(COATP)$_4$ and [CoPc(CO$_2$H)$_4$(COATP)$_4$@AgNPs], while Raman spectra of the Fe, Ni and Cu derivatives are reported in Tables 3 and 4, which summarize the positions of the main vibrational bands of all new compounds reported herein. In the Raman spectra of the various compounds, the vibrational modes below 600 cm^{-1} are generally attributable to the deformation vibration of the macrocyclic ring, the vibration of the metal-nitrogen bond, and the deformation vibration of the indole ring, all of which have relatively low intensities. The vibrational modes between 600 and 900 cm^{-1} are mainly due to the elongation vibration of the large ring and the deformation vibration of the benzene ring. The vibrational modes at approximately 1330 cm^{-1} are attributable to the C-H Raman vibrational modes of the

phthalocyanines.

The Raman band observed at approximately 247 cm^{-1} in the complexes is attributed to the metal-nitrogen stretching vibration. Indeed, the metal-nitrogen stretching vibration of several MPc has been analyzed based on far-infrared data [30]. The results are in good agreement with our assignment. The relative intensities of certain bands in the complex increase when it is associated with NPs compared to the complex alone. This includes, in particular, the intense band at circa 1500 cm^{-1} observed in the Raman spectra of the hybrid species [$MPc(CO_2H)_4(COATP)_4$@AgNPs], M = Fe, Co, Ni, Cu, a band corresponding to the vibration of the C-N-C bonds in the pyrrole group of the phthalocyanine macrocycle [31]. Lokesh K.S. et al., in their vibrational spectroscopic study of hybrid species composed of tetraamine cobalt phthalocyanine and silver (or gold) NPs [10], observed an increase in the intensity of certain vibrational bands, which they attributed to the SERS (surface-enhanced Raman spectroscopy) effect. This effect is specific to metal NPs exhibiting SPR (surface plasmon resonance) properties in the visible range, such as AgNPs [32-35]. The most intense band in the Raman spectrum, at circa 1500 cm^{-1}, varies considerably depending on the size of the metal ion center in the MPc complexes. This variation is, in fact, a good indicator of the effect of metal ions on changes in the Raman shift [30, 36]. As shown in Tables 3 and 4, the position of the Raman vibration band of the C-N-C bonds for the [$MPc(CO_2H)_4(COATP)_4$] series, M= Fe, Co, Ni, Cu, ranges from 1515 cm^{-1} for iron, 1522 cm^{-1} for cobalt, 1541 cm^{-1} for copper, and 1553 cm^{-1} for nickel, resulting in a shift of up to 38 cm^{-1} from Fe to Cu, observed due to the difference in metal ions. As for the hybrid species [$MPc(CO_2H)_4(COATP)_4$@AgNPs], the position of the C-N-C vibration band also varies depending on the central metal and follows the ascending order Fe (1516 cm^{-1}) < Co (1525 cm^{-1}) < Ni (1548 cm^{-1}) < Cu (1558 cm^{-1}). The shift in the C-N-C bridge linkages for amides and hybrid species followed the same pattern depending on the variation in the central metal ion, which is likely related to the radius and polarization strength of the central metal ion of the complexes [30].

For the iron-derived hybrid species, the small cationic radius induces a very strong polarization force. As a result, it can interact strongly with the phthalocyanine ring, causing the electrons in the conjugated ring system to move toward the central metal of the phthalocyanine ring and exhibiting a relatively strong ring contraction, which results in a relatively large Raman shift of all the vibrations bands [30].

The SERS effect observed in the spectra of the hybrid species supports the previous results obtained through IR analysis and confirms the synthesis of the [$MPc(CO_2H)_4(COATP)_4$@AgNPs] hybrids.

Table 3. *Characteristic Raman vibration bands in cm^{-1} of Feo and Co compounds.*

[$FePc(CO_2H)_4(COATP)_4$]	[$FePc(CO_2H)_4(COATP)_4$@AgNPs]	[$CoPc(CO_2H)_4(COATP)_4$]	[$CoPc(CO_2H)_4(COATP)_4$@AgNPs]	Attributions
1765	1765	1765	1762	C=O
	1660		1666	C=C
1599		1593	1603	
1515	1516	1522	1525	C-N-C
1437	1422	1428	1430	C=N
1349	1351	1351	1353	C-H
1330	1282	1311	1314	
1217		1215	1214	C-O
1201	1203	1177	1177	
1189		1114	1085	C-N
1086	1083	1064		
992	996	996	992	C-C
902	902	897	900	Vibrational-bending mode of the benzene ring
823	818	823	815	
742	739	740	741	
669	666	675	672	ν_{C-S} aryl
		622		

[FePc(CO$_2$H)$_4$(COATP)$_4$]	[FePc(CO$_2$H)$_4$(COATP)$_4$@AgNPs]	[CoPc(CO$_2$H)$_4$(COATP)$_4$]	[CoPc(CO$_2$H)$_4$(COATP)$_4$@AgNPs]	Attributions
582	582	581	586	
479	472	479	479	Vibrational-bending mode of the benzene ring; indole ring distortion; metal-nitrogen bond
392	398	398	398	
336	330	337	336	
284	279	284	280	
243	240	245	247	

Table 4. *Characteristic Raman vibration bands in cm^{-1} of Ni and Cu compounds.*

[NiPc(CO$_2$H)$_4$(COATP)$_4$]	[NiPc(CO$_2$H)$_4$(COATP)$_4$@AgNPs]	[CuPc(CO$_2$H)$_4$(COATP)$_4$]	[CuPc(CO$_2$H)$_4$(COATP)$_4$@AgNPs]	Attributions
1762	1765	1769	1763	C=O
1596	1610	1642	1593	C=C
		1588		
1541	1548	1553	1558	N-C-N
1440	1438	1442	1441	C=N
1356	1360	1352	1355	C-H
1325	1329	1321	1326	
	1205	1215	1218	C-O
1191	1190	1193	1178	
		1121	1115	C-N
1074	1072	1073	1061	
992	995	1000		C-C
909	902	900		Vibrational-bending mode of the benzene ring
	815	825	847	
741	744	741	742	
680	676	673	677	$\nu_{C\text{-}S}$ aryl
			622	
579	582	583	585	
480	474	483	485	
390	3998 +.+3	399		Vibrational-bending mode of the benzene ring; indole ring distortion; metal-nitrogen bond
326	340	336	335	
269	378	272		
235	246	245	245	
200	208	214	212	

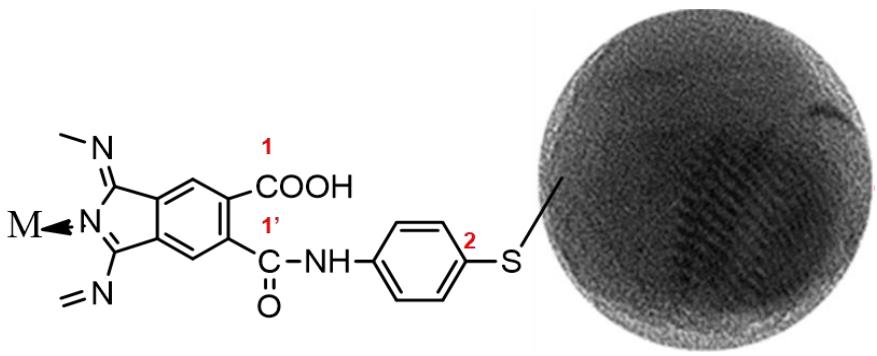
3.4. Solid-State ^{13}C Nuclear Magnetic Resonance (^{13}C NMR)

Solid-state NMR is a key tool for identifying surface species, particularly by elucidating the connectivity between atoms and other constituents. This involves measuring or detecting dipole or scalar coupling, which in particular has led to the development of CP-MAS solid-state ^{13}C NMR. Indeed, solid-state ^{13}C NMR suffers from low sensitivity, which is further exacerbated by the fact that surface species constitute only a small fraction of the sample. In such a situation, solid-state CP-MAS ^{13}C NMR can be a particularly well-suited tool, and it is generally used to gain a better understanding of the structure of polycrystalline powders, crystals, or insoluble compounds. When combined with the low solubility of MPcs, CP-MAS NMR emerges as an innovative tool for characterizing hybrid nanomaterials thereof [21]. The ^{13}C chemical shifts of the characteristic carbon atoms (Figure 10, top scheme) in Co, Ni, and Cu compounds are shown in Table 5.

Table 5. *^{13}C chemical shifts of the carbon atoms in Co, Ni and Cu compounds.*

	Chemical Displacements (ppm)	
Compounds	**Carbon 1-1' (C_{amid}, C_{acid})**	**Carbon 2 (C-ATP)**
$[CoPc(CO_2H)_4(COATP)_4]$	164	120
$[CoPc(CO_2H)_4(COATP)_4$@AgNPs]	165	126
$[NiPc(CO_2H)_4(COATP)_4]$	164	127
$[NiPc(CO_2H)_4(COATP)_4$@AgNPs]	165	131
$[CuPc(CO_2H)_4(COATP)_4]$	160	124
$[CuPc(CO_2H)_4(COATP)_4$@AgNPs]	167	126

The spectra of the MPc complexes of Co, Ni or Cu and nanohybrids thereof, together with their assignments, are shown in Figure 10, bottom. We did not record the spectra of the compounds containing iron due to its unique paramagnetic properties. In fact, studies of paramagnetic coordination complexes also show that iron complexes can be difficult to detect in solid-state ^{1}H or ^{13}C NMR, even when they are more readily detectable in solution, because certain anisotropic interactions are not sufficiently averaged out by MAS; which results in large shift anisotropies that otherwise generate overlapping side bands, making it difficult to interpret the NMR spectrum [37, 38].



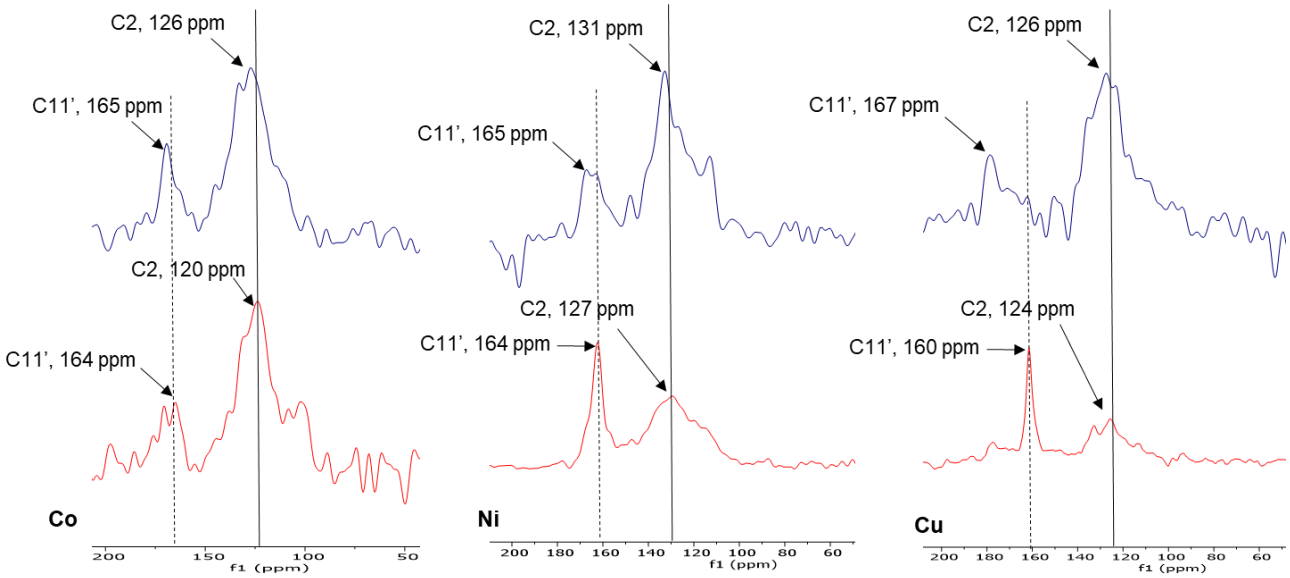


Figure 10. *Top, schematic representation of the key atoms studied in [MPc(CO$_2$H)$_4$(COATP)$_4$@AgNPs] hybrids and bottom, solid-state NMR ^{13}C CP-MAS spectra of [MPc(CO$_2$H)$_4$(COATP)$_4$] (red line) and [MPc(CO$_2$H)$_4$(COATP)$_4$@AgNPs] (blue line).*

In the case of Co, Ni and Cu, the use of the CP-MAS technique allows us to obtain spectra with good resolution, which facilitates the assignment of the various chemical shifts and the comparison of ^{13}C NMR spectra. The peak observed around 165 ppm (C11') could be attributed to the juxtaposition of the carbon signals of the acid (C1) and amide (C1') groups in the coordinated complexes. It is only slightly shifted in the spectra of the Co and Ni hybrids upon coordination of the complex to the NP surface. In contrast, the shift to the left of this peak is approximately 7 ppm in the spectrum of the Cu hybrid in comparison to the spectrum of the free Cu complex; This result is consistent with those reported in the literature [22, 23]. As for the carbon-2 peak, it is observed at 120, 127, and 124 ppm (Figure 9), respectively, in the spectra of the [M(CO$_2$H)$_4$(COATP)$_4$] complexes. These assignments were made by analogy to the results obtained by Toscano et al. [21] when they studied a series of MPc complexes using solid-state CP-MAS NMR. We observe that after hybrid formation, this peak is observed at 126, 130, and 126 ppm in the spectra of Co, Ni, and Cu, respectively. This shift has been reported in previous studies of Toscano et al. In fact, a de-shielding or shielding effect is observed on the α-carbon (directly bonded to sulfur) in an S-Ag bond in solid-state ^{13}C NMR spectra. It results primarily from an inductive electronic effect transmitted through the C-S bond, amplified by the nature of the Ag-S coordination.

The broadening and chemical shifts observed in the spectra of the hybrid compounds may indicate their formation. Furthermore, research in the literature [33] explains that in metal nanoparticles (particularly noble metals), conduction electrons have a dramatic influence on the resulting NMR spectra due to nuclear coupling with conduction electrons at the particle's surface, known as hyperfine coupling. It is well established that this hyperfine coupling of nuclear spins to unpaired conduction electrons in the metal produces a dramatic shift in the NMR frequency known as the Knight shift, first observed by W. D. Knight in 1949 [39] in metallic Li, Na, Al, Cu, and Ga, whose NMR resonance appears at a frequency different from that of the same element in a nonmetallic environment, and since then observed in many other metals among which silver [40].

Furthermore, for a carbon atom bonded via an S-Ag bond on the surface of a AgNP, radio frequencies can be absorbed by delocalized conduction electrons within the particle that interact via Fermi contact with nuclei near the surface (Ag itself, and, via partial transmission, S and C). It is this phenomenon that modulates the chemical shift (Knight shift) and the relaxation rate of the probed nuclei, providing a highly efficient nuclear relaxation pathway (accelerated T1 relaxation), a mechanism distinct from classical dipole relaxation. It is this electron-nucleus coupling that can result in broadened lines or signal loss, which could explain the results we obtained (Figure 10).

4. Conclusion

This work has made it possible to synthesize and characterize new nanostructured hybrid systems based on the combination of transition-metal phthalocyanines (of Fe, Co, Ni and Cu) and AgNPs. The originality of this approach lies in the dual functionalization of the phthalocyanine macrocycle.

The electronic absorption spectra clearly confirm the modification of the nanoparticle surface through the binding of the complexes. Similarly, the TEM images show good dispersion of the particles in solution.

Analysis by vibrational spectroscopy highlighted several key points. The infrared spectra confirmed an effective interaction between the amide complexes and the nanoparticles, marked in particular by a modulation of intensities and shifts

in characteristic frequencies, notably around 900 cm^{-1}. Variations in the central metal significantly influenced the metal-ligand vibrational modes and the electronic density of the macrocycle. Raman spectroscopy identified a SERS effect due to the plasmonic resonance properties of the AgNPs. The shifts observed for the C-N-C bond (up to 26 cm^{-1}) follow a clear trend related to the ionic radius and the polarizing power of the metals (Fe < Co < Cu < Ni).

The chemical shifts observed in the ^{13}C CP-MAS solid-state NMR spectra support the previously obtained results and suggest the formation of hybrid compounds.

The detailed understanding of metal coordination and surface interactions established in this study opens up promising avenues for optimizing these compounds, particularly in the development of next-generation antibacterial agents or highly sensitive photosensitizers.

The analysis of our results could make a significant contribution to understanding the behavior of these compounds and guide their intended applications.

Abbreviations

DMF	Dimethyl Formamide
DMSO	Dimethyl Sulfoxide
ATR	Attenuated Total Reflectance
UV	Ultraviolet
IR	Infrared
NMR 13C	Nuclear Magnetic Resonance of Carbon 13
TEM	Transmission Electron Microscopy
TMS	Tetramethylsilane

Acknowledgments

The authors thank the CNRS and the Paul-Sabatier University for their financial support, and the Raimond Castaing Microcharacterization Center for access to the microscopes. They would like to thank Joseph KI ZERBO University, Paul-Sabatier University and particularly the SCAC-French Embassy in Ouagadougou, Burkina Faso for their help in carrying out this work.

Author Contributions

Lassane Tarpaga: Conceptualization, Methodology, Writing – original draft, Writing – review & editing

Wend Kuny Guy Aristide Nitiema: Data curation, Investigation, Writing – original draft

Seydou Ouedraogo: Investigation, Methodology

Youssoufou Bakouan: Investigation, Methodology

Bintou Sessouma: Investigation, Methodology

Mabinty Bayo Bangoura: Conceptualization, Methodology

Catherine Amiens: Conceptualization, Methodology, Supervision, Writing – review & editing

Karifa Bayo: Supervision, Writing – review & editing

Conflicts of Interest

The authors declare no conflicts of interest.

References

[1] Rawling, T., Austin C., Buchholz F., Colbran S, B., McDonagh, A, M. Ruthenium phthalocyanine-bipyridyl dyads as sensitizers for dye-sensitized solar cells: dye coverage versus molecular efficiency. Inorganic Chemistry. 2009, 48 (7), 3215-3227. https://doi.org/10.1021/ic802087n

[2] Quintiliani, M., Garc á-Frutos, E, M., Gouloumis, A., V ásquez, P., Ledoux-Rak, I., Zyss, J., Claessens, C, G., Torres, T. Synthesis, Characterisation and nonlinear optical properties of two-dimensional octupolar systems based on phthalocyanine compounds. European Journal of Organic Chemistry. 2005, 18, 3911-3915. https://doi.org/10.1002/ejoc.200500271

[3] Armstrong, N, R. Phthalocyanines and porphyrins as materials. Journal of Porphyrins and Phthalocyanines. 2000, 4 (4), 414-417. https://doi.org/10.1002/(SICI)1099-1409(200006/07)4:4%3C414::AID-JPP247%3E3.0.CO;2-B

[4] Sakamoto, K., Ohno-okumura, E. Syntheses and functional properties of phthalocyanines. Materials. 2009, 2(3), 1127-1179. https://doi.org/10.3390/ma2031127

[5] Al-Raqa, S, Y. The synthesis and photophysical properties of novel, symmetrical, hexadecasubstituted Zn phthalocyanines and related unsymmetrical derivatives. Dyes and Pigments. 2008, 77(2), 259-265. https://doi.org/10.1016/j.dyepig.2007.05.002

[6] Hacivelioğlu, F., Durmuş, M., Yeşilot, S., Gürek, G, A., Kili ç A., Ahsen, V. The synthesis, spectroscopic and thermal properties of phenoxycyclotriphosphazenyl-substitued phthalocyanines. Dyes and Pigments. 2008, 79 (1), 14-23. https://doi.org/10.1016/j.dyepig.2007.12.010

[7] Gunseli, G., Yunus, P., Oguzhan, A., Semih, G. Investigation of photophysicochemical properties of peripheral tetra-substituted Zn(II) and Mg(II) phthalocyanine compounds containing thiol group, Journal of Molecular Structure, Volume 1336, 2025, 142021, https://doi.org/10.1016/j.molstruc.2025.142021

[8] Forteath, S., Antunes, E., Chidawanyika, W., Nyokong, T. Unquenched fluorescence lifetime for β-phenylthio substituted zinc phthalocyanine upon conjugation to gold nanoparticles. Polyhedron. 2012, 34(1), 114-120. https://doi.org/10.1016/J.POLY.2011.12.015

[9] Masilela, N., Antunes, E., Nyokong, T. Axial coordination of zinc and silicon phthalocyanines to silver and gold nanoparticles: An investigation of their photophysicochemical and antimicrobial behavior. Journal of Porphyrins and Phthalocyanines. 2013, 17(6), 417-430. https://doi.org/10.1142/S1088424613500016

[10] Lokesh, K, S., Narayanan, V., Sampath, S. Phthalocyanine macrocycle as stabilizer for gold and silver nanoparticles. Microchimica Acta. 2009, 167(1), 97-102. https://doi.org/10.1007/s00604-009-0226-3

[11] Mgidlana, S., Sen, P., Nyokong, T. Photodegradation of tetracycline by asymmetricalzinc(II)phthalocyanines conjugated to cobalt tungstate nanoparticles. Journal of Molecular Structure. 2022, 1261, 132938. https://doi.org/10.1016/j.molstruc.2022.132938

[12] Pinto, B, C, S., Ambrósio, J, A, R., Marmo, V, L, M., Pinto, J, G., Raniero, L, J., Ferreira-Strixino, J., Andreza, R, Simioni., Milton, Beltrame Jr. Synthesis, characterization, and evaluation of chloroaluminium phthalocyanine incorporated in poly(ε-caprolactone) nanoparticles for photodynamic therapy. Photodiagnosis Photodynamic Therapy. 2022, 38, 102850. https://doi.org/10.1016/j.pdpdt.2022.102850

[13] Nombona, N., Antunes, E., Litwinski, C., Nyokong, T. Synthesis and photophysical studies of phthalocyanine-gold nanoparticle conjugates. Dalton Transactions. 2011, 40(44), 11876-84. https://doi.org/10.1039/c1dt11151e

[14] Sen, P., Nyokong, T. Enhanced photodynamic inactivation of *Staphylococcus aureus* with Schiff base substituted zinc phthalocyanines through conjugation to silver nanoparticles. Journal of Molecular Structure. 2021, 1232, 130012. https://doi.org/10.1016/j.molstruc.2021.130012

[15] Tarpaga, L., Sessouma, B., Ouedraogo, S., Colliere, V., Bayo, B, M., Amiens, C., Bayo, K. Synthesis and study of the physicochemical properties of a hybrid species: Iron phthalocyanine-silver nanoparticles. Chemistry Africa. 2022, 5(4), 811-820. https://doi.org/10.1007/s42250-022-00400-w

[16] Bruna, T., Maldonado-Bravo, F., Jara, P., Caro, N. Silver nanoparticles and their antibacterial applications. International Journal of Molecular Sciences. 2021, 22(13), 7202. https://doi.org/10.3390/ijms22137202

[17] Suman, V., Airinei, A., Potlog, T. Synthesis of thiol-functionalized metal phthalocyanines-silver nanoparticles assemblies and their photophysics. Scientific Reports. 2026, 16, 26738. https://doi.org/10.1038/s41598-026-53029-x

[18] Lassane, T., Youssoufou, B., Seydou, O., Bintou, S., Mabinty, B, B., Catherine, A., Jerôme, E., Karifa, B. Synthesis of a hybrid nanomaterial combining silver nanoparticles with water-soluble zinc phthalocyanines [ZnPc$(CO_2H)_4$$(COATP)_4$@AgNPs]. Bulletin of the Chemical Society of Ethiopia. 2025, 39(4), 713-729. https://doi.org/10.4314/Bcse.V39i4.9

[19] Tarpaga, L., Ouedraogo, S, Nitiema, W, K, G, A., Sessouma, B., Bayo-Bangoura, M., Amiens, C., Esvan, J., Bayo, K. Synthèse et etude des proprietes physicochimiques d'un nouveau complexe de la phtalocyanine de zinc substitue à la peripherie: [ZnPc$(CO_2H)_4$$(COATP)_4$]. Journal of Ouest-African Chemistry Society; 2023, 52, 44-55. https://www.soachim.info/document/journal-soachim/article/Vol-052Num-1-8491dc750825caaa5a3c73f4c1765d10.pdf

[20] Chaikin, Y., Bendikov, T, A., Cohen, H., Vaskevich, A., Rubinstein, I. Phosphonate-stabilized silver nanoparticles: One-step synthesis and monolayer assembly. Journal of Materials Chemistry C. 2013, 1(22), 3573. https://doi.org/10.1039/c3tc30249k

[21] Toscano, P, J., Tobin, J, M. Electrically conductive metallomacrocyclic assemblies. High-resolution solid-state NMR spectroscopy as a probe of local architecture and electronic structure in phthalocyanine molecular and macromolecular "metals". Journal American Chemical Society. 1986, 108(3), 437-444. https://doi.org/10.1021/ja00263a013

[22] Nishiyama, Y., Fukushima, T., Fukuchi, M., Fujimura, S., Kaji, H. Sensitivity boosting in solid-state NMR of thin organic semiconductors by a paramagnetic dopant of copper phthalocyanine. Chemical Physics Letters. 2013, 556, 195-199. https://doi.org/10.1016/j.cplett.2012.11.043

[23] Pushkarev, V, E., Shulishov E, V., Tomilov, Y, V., Tomilova, L, G. The first example of a carbon label for interpreting the 13C NMR spectra of phthalocyanine metal complexes. Mendeleev Communications. 2007, 17(4), 218-219. https://doi.org/10.1016/j.mencom.2007.06.011

[24] Gadenne, V., Bayo-Bangoura, M., Porte, L., Patrone, L. Solvent induced aggregation of protoporphyrin and octacarboxylphthalocyanine of zinc deposited on gold surface. Journal of Colloid and Interface Science. 2011, 359(1), 47-55. https://doi.org/10.1016/j.jcis.2011.03.073

[25] Rapulenyane, N., Antunes, E., Nyokong, T. A study of the photophysicochemical and antimicrobial properties of two zinc phthalocyanine-silver nanoparticle conjugates. New Journal of Chemistry. 2013, 37(4), 1216. https://doi.org/10.1039/c3nj41107a

[26] Stuart, B, H. Infrared spectroscopy: fundamentals and applications. Wiley & Sons; 2004.

[27] Bao, M., Yongzhong, B., Llew, R., Rongming, W., Dennis, P, A., Changqin, M., Jianzhuang, J. Vibrational spectroscopy of phthalocyanine and naphthalocyanine in sandwich-type (na)phthalocyaninato and porphyrinato rare earth complexes: (Part 10) The infrared and Raman characteristics of phthalocyanine in heteroleptic bis(phthalocyaninato) rare earth complexes with decreased molecular symmetry. Vibrational Spectroscopy. 2004, 34(2), 283-291. https://doi.org/10.1016/j.vibspec.2004.01.002

[28] Kobayashi, T., Kurokawa, F., Uyeda, N., Suito E. The metal-ligand vibrations in the infrared spectra of various metal phthalocyanines. Spectrochimica Acta Part A: Molecular Spectroscopy. 1970, 26(6), 1305-1311. https://doi.org/10.1016/0584-8539(70)80036-8

[29] Aroca, R., Martin, F. Trace analysis of tetrasulphonated copper phthalocyanine by surface enhanced Raman spectroscopy. Journal of Raman Spectroscopy. 1986, 17 (3), 243-247. https://doi.org/10.1002/jrs.1250170303

[30] Zhang, X., Lin, W., Zhao, H., Wang, R. Raman spectra study of p-tert-butylphenoxy-substituted phthalocyanines with different central metal and substitution positions. Vibrational Spectroscopy. 2018, 96, 26-31. https://doi.org/10.1016/j.vibspec.2018.02.009

[31] Aroca, R., Clavijo, R, E., Jennings, C, A., Kovacs, G, J., Duff, J, M., Loutfy, R, O. Vibrational spectra of lutetium and ytterbium bis-phthalocyanine in thin solid films and SER(R)S on silver island films. Spectrochimica Acta Part A: Molecular and Biomolecular Spectroscopy. 1989, 45(9), 957-962. https://doi.org/10.1016/0584-8539(89)80154-0

[32] Losytskyy, M., Akbay, N., Chernii, S., Avcı, E., Chernii, V., Yarmoluk, S., Mustafa C., Vladyslava, K. Characterization of the interaction between phthalocyanine and amyloid fibrils by surface-enhanced Raman scattering (SERS). Analytical Letters. 2018, 51(2), 221-228. https://doi.org/10.1080/00032719.2017.1321655

[33] Walton, I, M., Cox, J, M., Benson, C, A., Patel, D, D, G., Chen, Y, S., Benedict, J, B. The role of atropisomers on the photoreactivity and fatigue of diarylethene-based metal-organic frameworks. New Journal of Chemistry. 2016, 40(1), 101-106. https://doi.org/10.1039/c5nj01718a

[34] Jiang, J., Bao, M., Rintoul, L., Arnold, D, P. Vibrational spectroscopy of phthalocyanine and naphthalocyanine in sandwich-type (na)phthalocyaninato and porphyrinato rare earth complexes. Coordination Chemistry Reviews. 2006, 250(3-4), 424-448. https://doi.org/10.1016/j.ccr.2005.09.009

[35] Zhang, Y., Zhang, X., Lu, Z., Xu, H., Jiang, J. Comparative density functional theory study of the structures and properties of metallophthalocyanines of group IV B. Vibrational Spectroscopy. 2006, 40(2), 289-298. https://doi.org/10.1016/j.vibspec.2005.11.004

[36] Bao, M., Wang, R., Rintoul, L., Arnold, D, P., Jiang, J. Vibrational spectroscopy of phthalocyanine and naphthalocyanine in sandwich-type (na)phthalocyaninato and porphyrinato rare earth complexes: Part 14. The infrared and Raman characteristics of phthalocyanine in “pinwheel-like” homoleptic bis[1,8,15,22-tetrakis(3-pentyloxy)phthalocyaninato] rare earth(III) double-decker complexes. Vibrational Spectroscopy. 2006, 40(1), 47-54. https://doi.org/10.1016/j.vibspec.2005.07.001

[37] Jan, N., Stanislav, K., Radek, M. Paramagnetic Effects in NMR Spectroscopy of Transition-Metal Complexes: Principles and Chemical Concepts. Accounts of Chemical Research. 2024, 57 (10), 1467-1477. https://doi.org/10.1021/acs.accounts.3c00786

[38] Koppe, J., Sanders, K, J., Robinson, T, C., Lejeune, A, L., Proriol, D., Wegner, S., Purea, A., Engelke, F., Clement, R, J., Grey, C, P., Pell, A J., Pintacuda, G. Resolving Structures of Paramagnetic Systems in Chemistry and Materials Science by Solid-State NMR: The Revolving Power of Ultra-Fast MAS. Angewandte International Editon Chemie. 2025, 64(1), e202408704. https://doi.org/10.1002/anie.202408704

[39] Knight, W, D. Nuclear Magnetic Resonance Shift in Metals, Physical Review Journals Archive. 1949, 76, 1259. https://doi.org/10.1103/PhysRev.76.1259.2

[40] Jang, Z, H. Investigation of the metallic property of noble metal nanoparticles with 1H solid-olid rticl Journal of the Korean Physical Society. 2022, 81(5), 428-433. https://doi.org/10.1007/s40042-022-00581-0